Regular Article

PHYSICAL CHEMISTRY RESEARCH
Published by the
Iranian Chemical Society
www.physchemres.org
info@physchemres.org

***Phys. Chem. Res.**, Vol. 2, No. 2, 202-216, December 2014.*
DOI: 10.22036/pcr.2014.5975

Design, Construction and Calibration of a Laser Ionization Time-of-Flight Mass Spectrometer

M. Tabrizchi*, H. Farrokhpour, F. Abyar, H. Azad, M. Mirian and V. ILbeigi
Department of Chemistry, Isfahan University of Technology, Isfahan, 84156-83111, IRAN
(Received 15 February 2014, Accepted 14 July 2014)

A time-of-flight mass spectrometer (TOF-MS) developed in our laboratory at Isfahan University of Technology is described here. The TOF-MS instrument uses laser as the ionization source which provides an opportunity to investigate the ions formed in laser ablation or desorption. The TOF-MS has an ionization chamber containing an accelerator and an ion lens to focus the ions into a one meter linear flight tube mass analyzer. Laser beam enters the ionization chamber through quartz window and can be focused either on the accelerator plates or in between. Solid sample may be deposited on the accelerator plate. Gas samples can also be admitted into the ionization chamber perpendicular to the accelerator axis through a leak valve. Mass spectra were obtained for gas samples as well as test solid samples. For the gas phase ionization, the laser was focused in the space between the accelerator plates while for the solid samples the laser beam was focused on the sample deposited on the repeller plate of the accelerator. Operational condition of the instrument were examined and mass calibration was achieved by measuring the flight time of the known alkali ions; Li^+, Na^+, K^+, Cs^+ and Rb^+. Ions of type $Alk^+(Alk.Halide)_n$ were observed for all alkali salts. In addition, spectra of alkali earth salts were obtained and assigned. An average mass accuracy of 0.016% was obtained and a mass resolution of 540 ($m/\Delta m$) was achieved for benzaldehyde (m/z = 106) as a test sample. The instrument is capable of being used for MALDI analysis.

Keywords: Time-of-flight, Mass spectrometry, Laser ionization, Alkali halides, Isotope pattern

INTRODUCTION

Time-of-flight (TOF) mass spectrometry (MS) is one of the most important analyzing techniques which works based on ionization and separation of ions in vacuum. It has the capability of detecting a wide range of chemical and biological substances through measuring the mass and fragmentation pattern of analytes. It also has a broad range of applications in physical and life sciences. The advantage of TOF instrument is that it can readily reach mass resolving power ($m/\Delta m$) of 1000-10000, with very high efficiency compared to other detection devices including magnetic sectors, quadrupole and ion traps. In addition, the very high upper-mass limit of TOF-MS has made it exclusive for high-mass applications, especially for bio-molecules and polymers, even up to 1,000,000 amu and greater.

*Corresponding author. E-mail: m-tabriz@cc.iut.ac.ir

CONCEPT OF TIME-OF-FLIGHT MASS SPECTROMETRY

Schematic diagram of a typical TOF mass spectrometer is shown in Fig. 1. For better understanding of the instrument and its working principle, the basic concept of time-of-flight mass spectrometry is reviewed here [1,7]. In time-of-flight mass spectrometer, ions of different masses are formed in an ionization region, extracted to a flight tube by an ion lens and are separated by their different flight times from the point of production to a plane of detection. A simple time-of-flight mass spectrometer consists of an acceleration region and a field free drift region. Ions are produced in the first region (the acceleration region), and are accelerated towards an ion collector through the second region (the field free drift tube). A detector at the end of the flight tube detects ions and a time-of-flight mass spectrum is obtained by recording the ion signal against time. For a

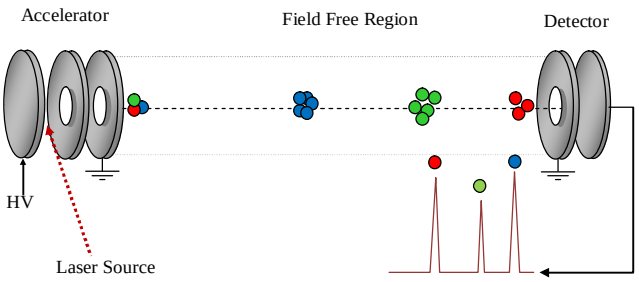

Fig. 1. Schematic diagram of TOF-mass spectrometer.

given acceleration field, the flight time depends on the mass-to-charge (*m/z*) ratio of the particle. Light ions move faster while heavy ions travel slower. The kinetic energy of the ion equals the potential energy that the ion feels in the electric field. Hence,

$$½\ mv^2 = qV \tag{1}$$

Design, Const Ruction and Calibration of a Laser Ionization

where m and v are mass and velocity of the ion, respectively, $q=ze$ is its charge and V is the potential in the acceleration region. The mass-to-charge ratio is obtained from the flight time and experimental parameters as:

$$\frac{m}{q} = \frac{2VT^2}{D^2} \tag{2}$$

where T and D are the flight time and flight length, respectively.

The ion arrival time depends on the initial ion energy plus the energy that the ion obtains from the electric field. The energy given to the ion by the electric field is not fixed for all ions as it depends on the position in which the ion is produced. However, if all ions of the same m/q value are formed at the same position in space with no initial velocity, their final energy would be equal and they would reach the collector at the same time. In practice, ions are produced at different positions in space and with different initial energies. The result is different total energy for ions of the same m/q value. This gives rise to different arrival times and thus peak broadening. To overcome the effect of an initial energy spread, a strong electric field is required. In a strong field, the initial ion energies will be much smaller than the energy given to the ions by the field. Thus, the ion energy spread is reduced and the resolution is improved. On the other hand, in a strong field the potential energy of ions depends very much on their position and any spatial distribution of ions will affect the ions arrival time and cause peak broadening. Therefore, a weak field is better to collect spatially distributed ions whereas a strong field reduces the effect of an initial energy spread. Wiley and McLaren suggested a two-field acceleration region in which two fields (usually one weak and one strong) can be independently optimized to give the best resolution [1]. Our instrument was built according to the design of Wiley and McLaren in which space focusing is achievable through adjusting electric fields to obtain best resolution.

The schematic diagram of the two-field time-of-flight mass spectrometer is shown in Fig. 2. In this diagram, the acceleration region consists of two parts. Ionization occurs in the first part and at the same time, electric field E_s is applied to the ions. The second acceleration region, with an applied electric field of E_d pushes ions into the field free region. The velocity of an ion (v) and the time (T) which spends in each part of the apparatus can be easily written down considering electrostatics and Newtonian mechanics, summarized as follows [1,7]:

$$v_o = v_o \tag{3}$$

$$v_1 = (v_o^2 + 2as_o)^{1/2} \tag{4}$$

$$v_2 = (v_o^2 + 2as_o + 2bd)^{1/2} \tag{5}$$

$$T_s = (v_1 - v_o)/a \tag{6}$$

$$T_d = (v_2 - v_1)/b \tag{7}$$

$$T_D = D/v_2 \tag{8}$$

where a and b are the ion accelerations in the first and second field regions, respectively, (see Fig. 2). The total flight time to the detector can then be written as:

$$T(v_o,s_o) = T_s + T_d + T_D \tag{9}$$

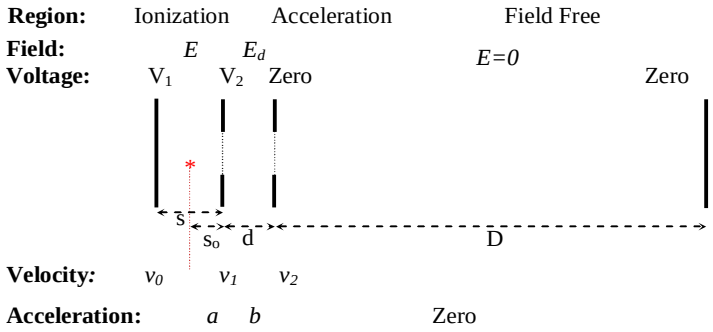

Fig. 2. A schematic diagram of the two field time-of-flight mass spectrometer. The asterisk represents the point where the ion is formed.

The acceleration *a*, can be calculated from Eq. (4) and substitution in Eq. (6) to give $T_s = 2s_o/(v_1+v_o)$. Similarly, using Eqs. (4, 5) and(6) gives T_d as $2d/(v_2+v_1)$. Substitution of these expressions in Eq. (9) gives the following equation:

$$T_{(\upsilon_o, s_o)} = \frac{2s_o}{\upsilon_1 + V_o} + \frac{2d}{\upsilon_2 + \upsilon_1} + \frac{D}{\upsilon_2} \tag{10a}$$

$$T_{(\upsilon_o, s_0)} = \frac{1}{\upsilon_2}\left(\frac{2s_o\upsilon_2}{\upsilon_1 + \upsilon_o} + \frac{2d\upsilon_2}{\upsilon_2 + \upsilon_1} + D\right) \tag{10b}$$

or

In most cases, the initial velocity is distributed over all directions in space and its average would be zero. In a specific case, if $v_o = 0$, the v_o is removed from Eq. (10), and the total flight time can be simplified using a new variable *k* which is defined as $(v_2/v_1)^2$. The factor $1/v_2$ can also be expressed in terms of the total energy of the ion, U_t as $1/v_2 = (m/2U_t)^{½}$. Therefore, the total flight time can be written as:

$$T_{(s_o)} = \left(\frac{m}{2U_t}\right)^{\frac{1}{2}}\left(2s_o\sqrt{k} + \frac{2\sqrt{k}}{\sqrt{k}+1}d + D\right) \tag{11}$$

Where *m* is the ion mass, U_t is the total ion energy in the flight region, s_o is the distance between the ion production point and the second electrode, and *d* is the separation of the second and third electrodes. *D* is the flight tube length and *k* is a variable, $(v_2/v_1)^2$, which is used for two-field systems. In one field systems $d = 0$ and $v_2 = v_1$, thus $k = 1$. The ion acceleration in an electric field, *E*, from Newtonian mechanics is *qE/m*, where *q* and *m* are the charge and mass of the ion, respectively. Substitution of *a* and *b* as qE_s/m and qE_d/m in Eqs. (4) and (5) and calculating the ratio $(v_2/v_1)^2$, gives *k* as:

$$k = \frac{dE_d}{s_o E_s} + 1 \tag{12}$$

Where E_s and E_d are the first and the second electric fields, as shown in Fig. 2. As $E_d=V_2/d$ *and* $E_s= (V_1-V_2)/s$, the *k* value can be written in terms of the applied voltages to the electrodes and distances,

$$k = \frac{V_2 s}{s_o(V_1 - V_2)} + 1 \tag{13}$$

The total ion energy, U_t, when $v_o = 0$, can also be written in terms of E_s, E_d, s_o and *d* as:

$$U_t = qs_oE_s + qdE_d \tag{14}$$

or in terms of voltages and distances,

$$U_t = q\left[\frac{s_o}{s}(V_1 - V_2) + V_2\right] \tag{15}$$

Substitution of Eq. (15) into Eq. (11) gives the total flight time as a function of instrumental parameters,

$$T_{(s_0)} = \left(\frac{m}{2q\left[\left(\frac{s_o}{s}\right)(V_1 - V_2) + V_2\right]}\right)^{\frac{1}{2}}\left(2s_o\sqrt{k} + \frac{2\sqrt{k}}{\sqrt{k}+1}d + D\right) \tag{16}$$

where V_1 and V_2 are the applied voltages to the first and second accelerator plate. s_o is the point where the ion is formed with respect to the second plate. *s, d,* and *D* are the first and second distance between the accelerator plate and the flight path, respectively, as shown in Fig. 2, and *k* is defined by Eq. 13. If a single-field accelerator is employed, where V_2 and *d* are zero and $k = 1$, Eq. (16) is simplified to:

$$T_{(s_o)} = \left(\frac{m}{2qV_1\left(s_o/s\right)} \right)^{\frac{1}{2}} (2s_o + D) \qquad (17)$$

It is further simplified to Eq. (2) if the ions are generated exactly at the first plate, *i.e.* the repeller, where $s_o = s$.

Space Focusing

Ions, in reality, are formed in different points (s_o) in the ionization region. The two-field acceleration scheme allows correcting for different initial positions and focusing the ions in space on the detector. Consider two ions with the same mass, formed in different positions, separated by a distance Δs_o, both with zero initial energy. The first ion which is farther from the flight tube detector by Δs_o, is expected to have a delay in its flight-time with respect to the second ion which is closer to the detector. However the first ion will gain a higher energy than the second one from the electric field because of its position. This increases the final velocity of the first ion and shortens its flight time. The idea of space focusing is that these two effects compensate each other so that the two ions of the same mass reach the collector at the same time.

Figure 3 shows space focusing at a plane at a distance *D*. This condition can be satisfied when $\partial T/\partial s_o$ from Eq. (16), is set to zero at $s_o = s/2$ [1]. This results in

$$D = s\,k^{3/2}\left(1 - \frac{2d}{s(k + \sqrt{k})}\right) \qquad (18)$$

D is the spatial focal length of the ion lens and $2s_o$ and *d* are the length of the first and the second field region, respectively (see Fig. 2). In deriving equation (18) it should be remembered that *k* in equation (16), is a function of *s* (see equations (12) and (13)). Also because the coefficient of *d*, in equation (16) changes between 1 and 2, when *k* goes from 1 to infinity, it is not very *s* dependent and is assumed constant. If *s, d* and *D* are fixed, then *k* is determined by Eq. (18) and therefore E_d/E_s , derived from Eq. (12), can be adjusted to give focusing at a particular distance *D* along the flight tube.

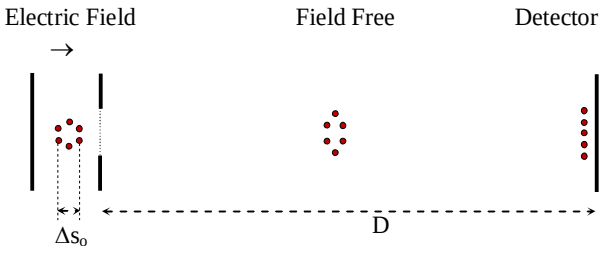

Fig. 3. Illustration of space focusing of spatially distributed ions, to a plane at distance *D*.

Resolution

Resolution in a TOF mass spectrometer is defined as the ratio $m/\Delta m$, where *m* is the ion mass and Δm is the peak width in mass units. As long as Δm is less than one amu, adjacent mass peaks are resolved. However, when the peak width is about 1 amu, the limit of resolution is reached and then $m/\Delta m$ corresponds to the largest resolvable mass, Max.(*m*), for which adjacent masses are completely separated. The ratio $m/\Delta m$ can be expressed in terms of time through Eq. (16). During an experiment, everything in Eq. (16) except *T* and *m* is constant, neglecting changes in initial energy. Therefore, the total flight time is proportional to $m^{1/2}$and equation (16) can be simplified to:

$$T = C\,m^{½} \qquad (19)$$

Differentiation of the logarithm of Eq. (19) gives:

$$m/\Delta m = ½(T/\Delta T) \qquad (20)$$

ΔT is the peak width which mainly depends on two factors, the initial energy distribution and the spatial distribution of the ions in the ionization region. Initial pulse width of the ion source is also important. Laser produces short pulses in the order of few nanoseconds which is appropriate for TOF mass spectrometry. The peak broadening due to the spatial distribution can be approximated by a Taylor expansion about s_o, *i.e.*,

$$\Delta T_{(\Delta s_o)} = \left(\frac{\partial T}{\partial s_o}\right)_{s_{/2}} \Delta s_o + \frac{1}{2}\left(\frac{\partial^2 T}{\partial s^2}\right)_{s_{/2}} \Delta s_o^{\,2} + \cdots\cdots \quad (21)$$

The first term in this equation was set to zero to satisfy the space focusing condition. The second term can be evaluated from equation (16) and to a good approximation the other terms can be neglected. A measure of spatial resolution can now be found by dividing T, from Eq. (11) by $\Delta T_{(\Delta s)}$ from Eq. (21). The result is [1];

$$M_{(\Delta s)} = m/\Delta m \approx 4k(s/\Delta s_o)^2 \quad (22)$$

In this equation, $m/\Delta m$ is the mass resolution considering only the initial spatial distribution effects. In reality, the initial kinetic energy of the ions formed in the ion source is not zero.

In general, the ion kinetic energy will be distributed in all directions. To investigate this effect on resolution, consider two ions with the same mass formed in the same position and having the same initial velocity but moving in opposite directions, towards and away from the collector. The delay time due to the initial velocities of the two ions, $\Delta T(v_o)$, will be the turn-around time of the ion moving away from the detector and can be considered as:

$$\Delta T(v_o) = 2v_o/a = 2mv_o/qE_s \quad (23)$$

This can be derived using the equation $v = at - v_o$, with the acceleration a written as qE_s/m and noting that at the turn-around point the ion velocity v is zero. To a good approximation, in Eq. (11), the flight time in the acceleration region can be neglected when D is large relative to d and s. In this case Eq. (11) can be shortened to give the flight time as $T = D\,(m/2U_t)^{1/2}$. Dividing T from this relation by $\Delta T(v_o)$ from Eq. (23), gives the ratio $T/\Delta T(v_o)$ as:

$$\frac{T}{\Delta T_{(v_o)}} = \frac{DqE_s}{2\sqrt{2mU_t}\,v_o} \quad (24)$$

Remembering that $m^{1/2}v_o = (2U_o)^{1/2}$, the mass resolution $m/\Delta m = \frac{1}{2}\,(T/\Delta T)$ becomes

$$\frac{m}{\Delta m_{(v_o)}} = \frac{1}{8}\frac{DqE_s}{\sqrt{U_t\,U_o}} \quad (25)$$

Equations (13) and (14) give the mass resolution, only from the initial energy distribution as:

$$M_{(v_o)} = \frac{m}{\Delta m_{(v_o)}} = \frac{1}{4}\left(\frac{U_t}{U_o}\right)^{\frac{1}{2}}\frac{D}{s}\frac{1}{k} \quad (26)$$

where U_t is the total energy of the ion, U_o is its initial value, s is the length of the first field region and D is the length of the flight tube.

This equation shows that a long flight tube and a short acceleration length, (s), is better for resolution. Another factor which determines resolution arising from an initial energy distribution is the ratio U_t/U_o. This factor can be increased by either increasing U_t; *i.e.*, increasing the voltage applied to the plates, or reducing U_o. An effective method to minimize the initial energy is using a supersonic molecular beam which causes a decrease of molecular internal energy [2]. There are also other methods to overcome the initial energy problem, such as time-lag-focusing, [1] in which a delay is applied between the ion formation and ion extraction to allow the ions to spread out in the ion source. In a case that ions of the same mass differ in absolute initial energy, the most effective method of energy focusing is the use of a reflectron, a very important development in the field of time-of-flight mass spectrometers [3-6].

INSTRUMENT DESIGN

The main purpose of this work was to have a time-of-flight mass spectrometer to detect ions formed by laser ionization. The design is similar to a TOF instrument used for recording the Resonance Enhanced Multi-photon Ionization (REMPI) spectra of some short lived molecules [7]. For reasonable resolution (~200) a flight tube of length of about one meter was chosen and the other parts were designed to be compatible with this flight tube length. The instrument was designed to accept solid samples as well as gaseous samples to be ionized *via* multiphoton ionization. A photograph of the instrument is shown in Fig. 4 [8]. The ionization source of the set-up is laser radiation produced by a Nd-YAG laser (Quantel model YAG980,France). The fundamental (1064 nm) and harmonics of the laser, 532 and 355 nm were all used for desorption and ionization.

The spectrometer consists of two parts, an ionization chamber and a mass analyzer chamber. On one side of the

Fig. 4. Photograph of the time-of-flight mass spectrometer, constructed in Isfahan University of Technology.

ionization chamber a convex lens is mounted to focus the laser radiation inside the chamber. Gas sample enters the chamber from the top through an inlet system. An ion lens is mounted inside the ionization chamber to extract the ions produced by laser into the mass analyzer via a small hole ≈ 2 mm in diameter. Both the ionization chamber and the mass analyzer chamber are separately pumped by turbomolecular pumps.

Ionization Chamber and Flight Tube

The ionization chamber is a cylindrical stainless steel chamber with several flanges which are used for the laser, the gas inlet, feed throughs, the turbomolecular pump and the flight tube. Two UV grade, fused silica optical window were mounted on both sides of the chamber to allow the laser beam into the center of the ionization region. A Plexiglas window was fixed on one side of the chamber, at 90^{o} with respect to the laser beam to see inside the chamber during the operation.

The flight tube is a one meter stainless steel tube with appropriate flanges on both sides. Two pairs of parallel plate electrodes were mounted horizontally and vertically, inside the flight tube to allow steering of the ion beam.

The Vacuum System

Two full range pressure gauges (Pfeiffer) were installed to read the pressure inside the ionization and the flight tube, separately. The ionization chamber is pumped by a 345 l s^{-1} turbomolecular pump backed by a 25.7 $m^3 h^{-1}$ rotary pump.

The ultimate background pressure was about 10^{-7} mbar which rose to 5×10^{-6} mbar during normal operation with solid sample and to 10^{-4} when gas sample was flowing. The flight tube was pumped separately by a 145 ls^{-1} turbomolecular pump backed by a 9.7 $m^3 h^{-1}$ rotary pump. The connection point between the two chambers is a 2 mm aperture hole to minimize gas passing into the flight tube. There was no pressure rise in the flight tube when gas samples were flowing. The flight tube chamber was maintained at a pressure of ~ 10^{-6} mbar during all experiments.

The Ion Lens

There were some spatial restrictions in the ion acceleration region which needed to be considered. For example, the first two electrodes should be separated sufficiently to allow the gas sample to pass through without collision with the lens plates. Also, the spacing should be enough to allow the laser beam is focused on the repeller plate. On the other hand, the plates cannot be too far apart, as the electric field produced will then not be uniform and will be perturbed by the assembly rods on which the lens is mounted.

Considering the above limitations, *s* and *d* were both set to 12 mm, respectively. The ion lens is a two-field design and consists of several circular plates. All electrodes were 50 mm in diameter and were supported on four stainless steel screwed rods covered by Teflon tubing, spaced apart by Teflon spacer which had been carefully and precisely cut. The diameter of the electrodes is more than twice the distance between them and protects the electric field from side penetrations of the rods which are grounded. The first plate (the repeller) was held typically at about +2.31 kV, with respect to the earth, and the second plate was held at zero Volts when solid sample was used and or whatever necessary for gas samples, to reach the space focusing at the detector, as described in section 2.1. The last plate was earthed and a chain resistor was connected between the plates; from the second to the last. This assembly provides a reasonably smooth field in the central area of the ion lens. To allow focusing of the ion beam, a focus lens was used. It consists of a cylindrical electrode, 10 mm length and 10 mm internal diameter, mounted between two grounded electrodes. Except for the repeller, all plates have an 8 mm diameter hole. The whole ion lens is mounted on an aluminum base, fixed to the ionization chamber.

The Sample Introduction and Inlet System

The gas inlet system (Fig. 5) consists of a leak valve, a stainless steel tube, connected to a Teflon tube which delivers the gaseous sample on top of the ion lens between the first and the second plates. The end position of the Teflon tube relative to the ion lens is adjustable to allow delivering enough gas above the photon beam. However, end of the tube was held further than ~1 cm above the laser focus. Solid sample was coated on the repeller of the accelerator and was directly irradiated by the laser light (see Fig. 5). To deposit solids, such as alkali salts, one drop of 5% solution were loaded to the repeller plate and let to dry. In order to avoid memory effect and contamination, a separate aluminum foil was used and replaced for each sample. The ionization chamber was opened when a fresh sample needed to be loaded. Then, the chamber was evacuated for an hour to reach the low vacuum conditions.

Power Supplies

Six home-made DC power supplies were used in the instrument; two (200-3000 V) for acceleration, one (0-50) for focusing and two (0-500) for deflection plates. Another high voltage power supply (200-4000 Volts) was used to drive the MCP detectors. All power supplies were mounted in a Rack below the spectrometer.

Detector and Signal Processing

To detect ions, channel plates (MCP) were mounted at the end of the flight tube. A 5.8 MΩ resistor was placed in parallel with the channel plates to allow an electric current to flow. The channel plates are typically biased at -3 kV. Due to the large potential drop, positive ions that impinge on these plates from the flight tube will be accelerated and will eject some electrons. In the channels, each electron, under collision with the walls, ejects several electrons because of the nature of the semiconductor and the strong electric field in the channels. Therefore, the number of electrons increase rapidly and amplification is achieved. The gain of this system depends on the applied potential and with the above voltage settings it is about 10^7. A simple copper plate, known as a Faraday plate, collects the electrons and then the signal is monitored by a digital storage oscilloscope. The signal is monitored by a fast Digital Oscilloscope (500 MS/s) which is triggered by a photodiode excited from the laser. The oscilloscope is linked to a computer *via* a USB interface. A computer program in connection with the oscilloscope was used for data acquisition and displaying the time-of-flight spectrum on the computer screen. Data were then further processed using common software such as Igor and Sigmaplot. The laser was running on 10 Hz repetition rate. Each laser pulse resulted in a complete spectrum, hence 10 spectra per second. To enhance the signal to noise ratio, a number of spectra were averaged.

EXPERIMENTAL

TOF Operation

To achieve space focusing, if D, d and s are fixed, the ratio of E_d/E_s or k is determined by Eqs. (18). In this case with

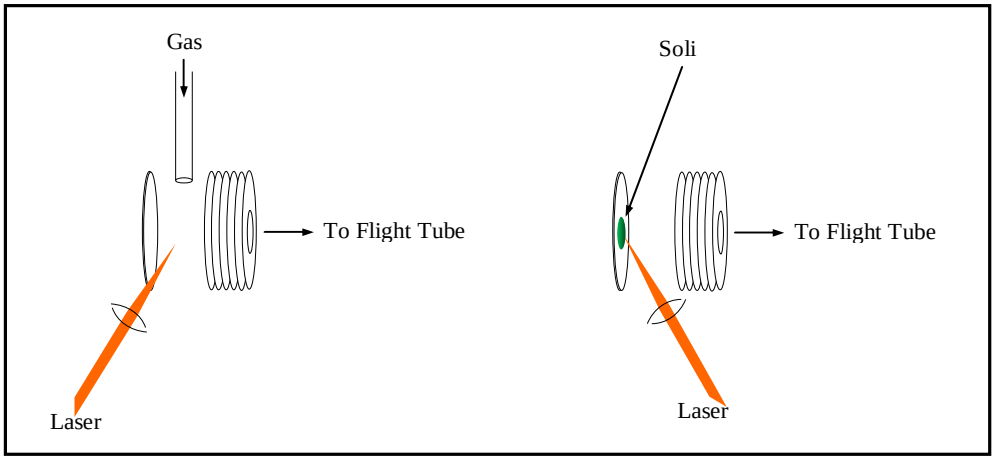

Fig. 5. Schematic diagram for the two sample introduction systems for gas and solid.

$D \approx 1$ m and $d = s = 12$ mm (see Fig. 2), k would be about 20. This means that to focus an ion beam on the channel plates at 1 mm distance from the ion lens, a value of 0.9 is required for the ratio V_d/V_r as $dE_d = V_2$ and $sE_s = (V_1 - V_2)$ resulting in $V_2/V_1 = (k - 1)/(k + 1)$. In initial experiments, attempts were made to satisfy this requirement of focusing at $k = 20$ and well resolved spectra were obtained. However, it was later realized that for low k values, such as $k = 3$, the resolution is still reasonable. This behavior is probably due to the very small size of the ionization volume when ions are made by multi-photon ionization using a focused laser beam for gas sample. The focus size is in the order of few μm. If Δs_o in Eq. (22) is assumed to be the size of the focal point, approximately 10^{-6} m, the calculated maximum resolved mass from the space contribution, even for very low k, is very large. Therefore, there is little contribution in the overall experimental resolution in this instrument from space focusing and it can be considered negligible. In fact, other factors such as the initial ion energy and repulsion, coming from the space charge, are more important in this instrument in determining resolution.

Also when solid sample is used, the ionization occurs in a plane at the repeller plate where $s_o = s$ and the two-field scheme is no longer applicable, thus $k = 1$. Hence, the initial energy of the ions, obtained from interaction with the laser beam determines the resolution. In the instrument, the flight tube length, D, relative to the ion lens length is large enough to apply Eq. (26). An estimate of the contribution to mass resolution from an energy distribution, for ions with 1 eV at initial kinetic energy, (the thermal kinetic energy at room temperature is about 0.04 eV), assuming the total energy, $U_t = 1000$ eV and $k = 1$, would be about 600. However, as mentioned before, the expected resolution would be less because of other factors such as space charge. In MPI this effect is important because of the very small size of the ionization volume and it becomes more important when the laser power is high. Also in the case of surface ionization, ions are formed in a very thin slice in the vicinity of the surface. Hence, the space charge in the direction of the flight path would also be important for solid samples. In addition, inhomogeneity of the electric field in the acceleration region, due to surface roughness and deviation from parallel structure of the plates, causes the ions to be spread over time.

TOF Spectra

As an example, the time-of-flight mass spectrum of benzaldehyde recorded using the laser ionization source at a wavelength of 355 nm, focused between the plates, is shown in Fig. 6. Benzaldehyde vapor was introduced into the chamber *via* the leak valve provided in the inlet system. The spectrum shows a number of mass resolved peaks including fragments of hydrogen, carbon, carbon dimer as well as the molecular ion at 106 amu. Expanded parts of the time-of-flight spectrum demonstrate that the mass peaks are clearly separated and the signal to noise is reasonable (21, for the most intense peak and 2 for the smallest peak versus back ground noise). Due to sharp signal, ringing effect is observed which is due to impedance mismatch between the collector and the signal cable. This needs to be improved.

The ionization energy of benzaldehyde is 9.5 eV [9] while the photon energy at 355 nm is only 3.5 eV. Observation of M^+ ion reveals that the ionization has happened via multi-photon absorption followed by ionization. At least, three photons have been involved in the ionization of benzaldehyde. Obviously, the process is not resonance but the laser power is so high to produce fragment ions, even hydrogen and carbon ions. Reducing the laser power or defocusing the beam resulted in less fragmentation.

A laser as an ionization source can provide variable fragmentation. Soft or hard ionization is achievable using different laser powers with different frequencies. A high laser power at short wavelengths is expected to lead to a considerable fragmentation of molecules such as hydrocarbons. The presence of many mass peaks in the time-of-flight spectrum suggests a hard ionization through a non-resonant multi-photon absorption. The laser wavelength can be scanned over a wide range, to observe the fragmentation pattern and relative intensities or to perform resonance enhanced multi-photon ionization (REMPI) spectroscopy.

The time-of-flight spectrum of RbCl salt as a solid sample, recorded with the laser TOF-MS instrument, is demonstrated in Fig. 7. To do this experiment, 20 μl of 5% RbCl solution was loaded onto an aluminum foil and after drying was mounted adjacent to the repeller plate. Alkali salts are easily ionized to alkali ions *via* thermal ionization when heated on a plate connected to a positive potential [10]. Laser provides the energy for surface ionization of the alkali salts. In this spectrum, three main ions, Na^+, K^+ and Rb^+ ions are observed in Fig. 7, where the Rb^+ is the strongest. The presence of K^+ and Na^+ ions is due to impurities in the RbCl salt. Clearly, all

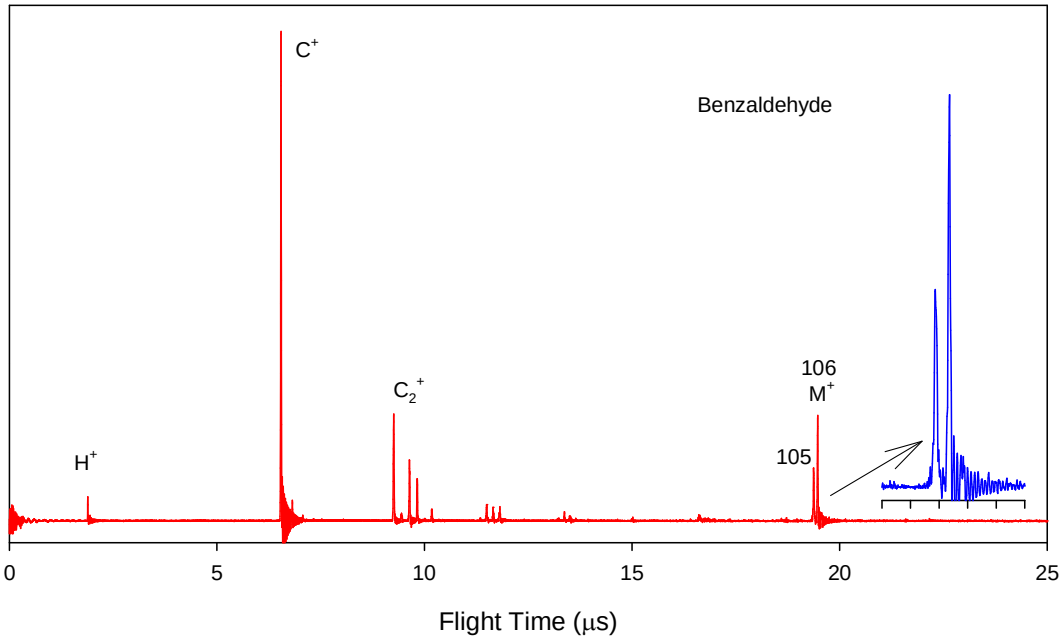

Fig. 6. TOF mass spectrum of benzaldehyde in gas phase, recorded at 355 nm laser wavelength.

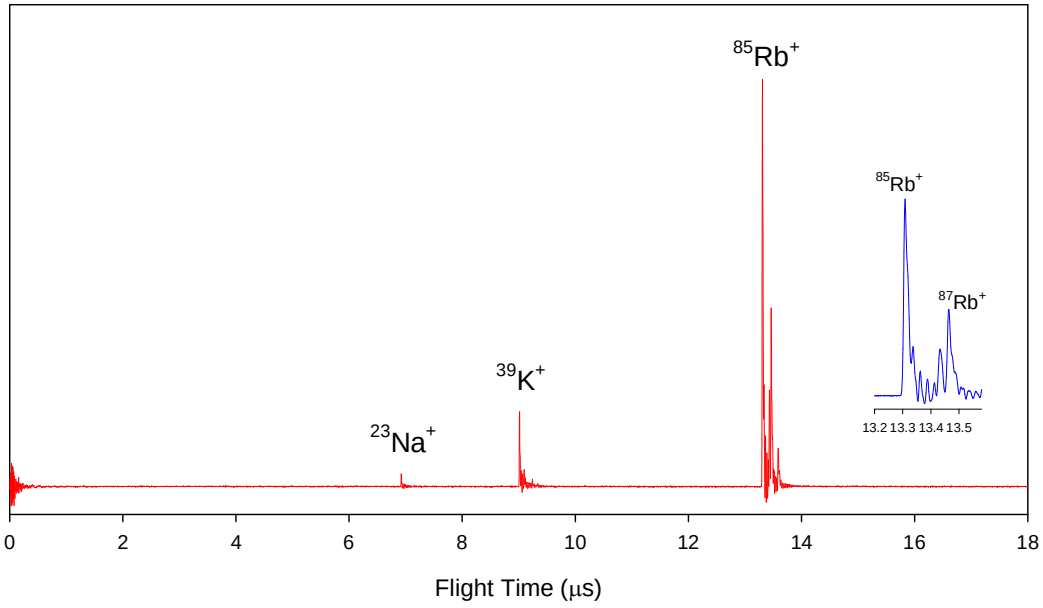

Fig. 7. TOF mass spectrum of RbCl saltas solid sample recorded with the laser TOF-MS.

mass peaks are well resolved as shown in the expanded part for the two Rb isotopes.

TOF mass spectra of different alkali salts were also recorded. For all alkali salts cluster ions of the type $A^+(AX)_n$, where A and X stand for alkali and halide, respectively, were observed. As an example, the time-of-flight spectrum of NaCl is shown in Fig. 8.

Isotope Ratio and Isotope Pattern

Some elements have more than one stable isotope with considerable abundance, such as potassium, chlorine and rubidium. Mass spectrometer is expected to separate different isotopes since they differ in mass. The two isotopes of potassium, ^{39}K and ^{41}K are fairly visible in Fig. 7. The two isotopes of rubidium, ^{85}Rb and ^{87}Rb with abundances 72.1% and 28.9%, respectively [11,12] are clearly separated in the mass spectrum of RbCl in Fig. 7. The presence of isotopes and their relative intensities often help to assign the mass peaks. Chlorine, for example, has two stable isotopes which differ by 2 amu with relative abundances 3:1. Hence, two adjacent peaks with 3:1 relative intensity, reveals the presence of chlorine. This is the case for the two $Na^+(NaCl)$ peaks at 81 and 83 amu in Fig. 8. Calcium and barium have many stable isotopes. In order to investigate the instrument response to different isotopes and to compare the isotope pattern, time-of-flight mass spectra of alkaline earth salts including $CaCl_2$, $BaCl_2$ and $SrCl_2$ were also recorded using laser ionization source. An example is shown in Fig. 9. Generally, the spectra contained ions of AE^+ and $AECl^+$, where AE stands for alkaline earth. The isotope pattern were simulated (width = 0.4 amu) considering the natural abundances of the stable isotopes and compared with the experimental spectra, as demonstrated in Fig. 9. Barium itself has 7 stable isotopes. These isotopes, in combination with chlorine having two stable isotopes, make 14 different combinations. The combined species are tabulated in Table 1, with their relative probabilities obtained through product of the relative abundances of the corresponding pair of isotopes. Due to small probability, some of the species in Fig. 9 will not be observed. Five peaks for Barium and seven peaks for $BaCl^+$ are observed in Fig. 9. The solid lines show the simulated pattern for all $BaCl^+$ with different isotopes, taking into account the relative population distributed by a Gaussian function for each peak. The simulated spectrum agrees very well with the experimentally recorded mass spectrum.

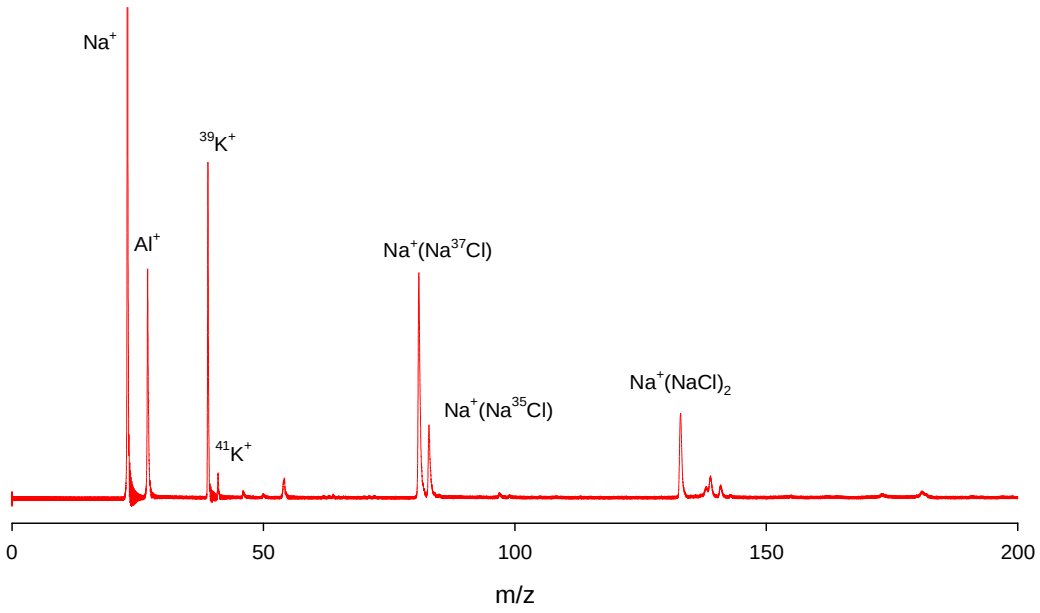

Fig. 8. Laser TOF-Mass spectrum of NaCl.

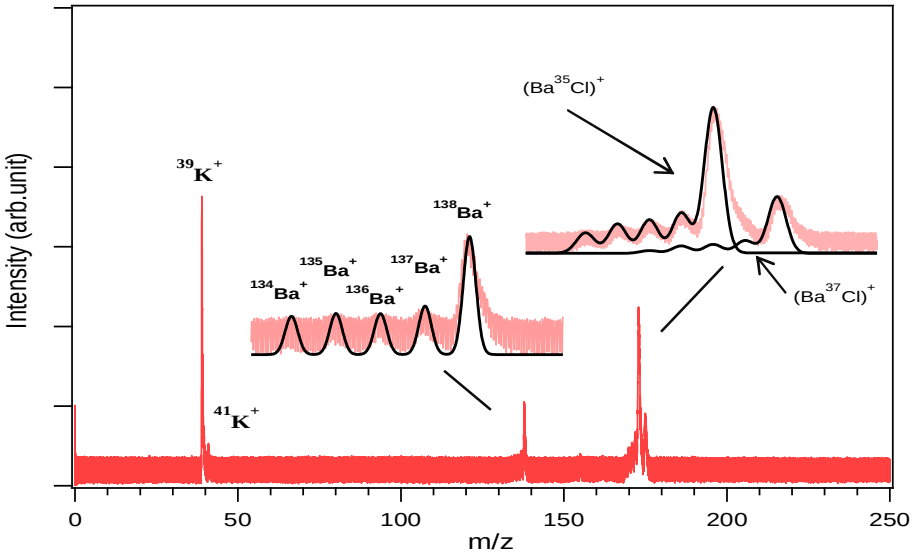

Fig. 9. Laser TOF-Mass spectrum of $BaCl_2$ along with the simulated spectra.

Table 1. Different Isotopes for $BaCl^+$ ion with their Relative Abundances

.

Compound	Nominal mass	Abundance (%)
$^{130}Ba^{35}Cl$	165	0.0803
$^{132}Ba^{35}Cl$	167	0.0765
$^{130}Ba^{37}Cl$	167	0.0257
$^{134}Ba^{35}Cl$	169	1.8314
$^{132}Ba^{37}Cl$	169	0.0245
$^{135}Ba^{35}Cl$	170	4.9948
$^{136}Ba^{35}Cl$	171	5.9510
$^{134}Ba^{37}Cl$	171	0.5856
$^{137}Ba^{35}Cl$	172	8.5090
$^{135}Ba^{37}Cl$	172	1.5972
$^{138}Ba^{35}Cl$	173	54.3271
$^{136}Ba^{37}Cl$	173	1.9030
$^{137}Ba^{37}Cl$	174	2.7210
$^{138}Ba^{37}Cl$	175	17.3729

Mass Calibration and Peak Assignment

Any mass spectrometer needs to be calibrated in order to measure accurate masses for identifying unknown species. The mass calibration of an unknown spectrum is usually a multistep process. Several methods exist for calibration before the final mass calibration is reached. The laser ionization TOF mass spectrometer was calibrated in traditional way with standard masses. Alkali cations Li, Na, K, Rb and Cs were

used for calibration. Alkali elements are easily ionized *via* thermal or surface ionization with the laser irradiated on the surface containing alkali salts. To cover a wide range of masses, five alkali chlorides were mixed in ratio of approximately 20:10:5:2:1 for the Li to Cs series, respectively. The mixing ratios were chosen to compensate for different ionization yield of the alkali elements. The result is demonstrated in Fig. 10, where alkali ions and their combination with chlorine are observed.

The first step was to get a rough mass calibration assuming that each peak is approximately at integer mass. Five known masses, 7, 23, 39, 85 and 133 for Li, Na, K, Rb and Cs, respectively were first considered. Based on Eq. (19), the total flight time is directly proportional to the square root of mass with zero intercept. A pre-calibration curve was obtained through plotting the flight time of the 5 known alkalis versus the square root of integer masses. The initial values for a and b in calibration equation $T = a(m/z)^{1/2} + b$, obtained from the first step was then used to guess the mass for other peaks. Based on the calculated approximate masses, other peaks were assigned. All combinations with general formula $A_nB_mCl_k$ where A and B could be any alkali cation and n, m and k each equals 0, 1 or 2, were examined. Isotope patterns were also considered and the peaks were assigned to the ions of type $A^+(BCl)$. Finally, the flight times were plotted against the exact masses and fitted to the linear function. The plot is shown in Fig. 11 that gives more accurate a and b. The points fit very well to a straight line, (correlation $r^2 = 0.99999989$) and the intercept is very close to zero (only 60ns on the mass-time axis) confirming correct mass assignment. The non-zero intercept is due to the delay in the electronic and data acquisition devices.

Mass Accuracy

Accurate mass is the experimentally measured mass value while exact mass is the calculated mass based on adding up the standard masses of each atom in the molecule. Exact mass differs from the integer mass or nominal mass. The integer mass for Na is 23 while its exact mass is 22.9803. Mass defect is the difference between the integer mass and the exact mass. By definition, only carbon atom has an exactly the same value for the exact and the integer mass which is 12, *i.e.* zero mass defect. Mass error is the difference between experimentally measured mass and the exact mass. Mass accuracy is then calculated through dividing the mass error by the exact mass and is expressed in percent or ppm unit. Mass accuracy is a great tool for target quantification and confirmation. Nowadays, high

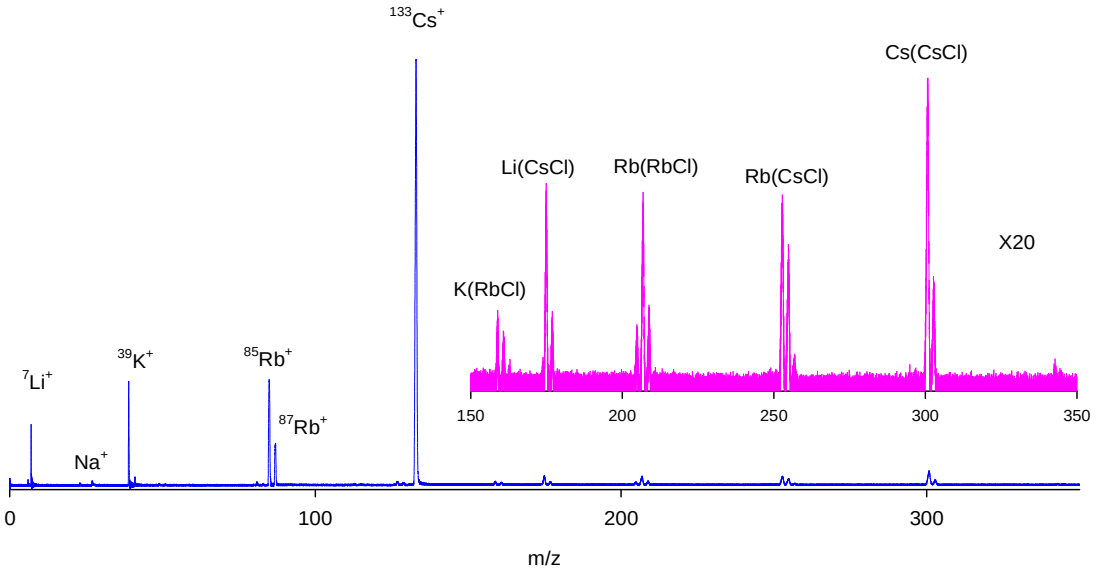

Fig. 10. Laser TOF-Mass spectrum of a mixture of all alkali chlorides.

resolution commercial TOF mass spectrometers with mass accuracy, as good as 0.5 ppm is available. We calculated accurate masses for the assigned species measured by the laser-TOF instrument, using Eq. (27) and the fitting parameters, *a* and *b*, obtained from the plot in Fig. 11. The results are tabulated in Table 2.

$$\frac{m}{z} = \left(\frac{T-b}{a}\right)^2 \qquad (27)$$

The mass errors are in the order of $\pm 10^{-2}$ which is very reasonable. The best mass accuracy is 0.0002% and if Aluminum is ignored the least accuracy is only 0.05% which is acceptable for elemental and small molecules analysis. The average mass accuracy is 0.016%.

Resolution

Analysis of the time-of-flight spectra, shown in Figs. 6 and 7, shows that the mass resolution is acceptable for the purpose that the instrument was designed. The full width at half maximum of the fastest moving ion, (H^+) is only 9 ns. This short time is comparable to the pulse duration of the laser pulse. This shows that we have reached a situation that the peak width is limited by the initial ion packet width created by the laser. The peak width increases to only15 ns for m/z = 300. The mass resolution, $M = m/\Delta m$, is about 390 for mass 300. This means that the maximum resolvable mass, M, where Δm = 1, would be about 300 amu. Even better resolution of 540 was observed for the 106 amu peak in benzaldehyde spectrum shown in Fig. 7. This spectrum was recorded when the laser was focused in gas phase between the two accelerator electrodes. With this geometry, space focusing was possible through adjusting the potential applied to each electrode, V_1 and V_2, (see Fig. 2). The experimental resolution of 390 is close to the theoretical value and it is very good for a linear TOF mass analyzer. Certainly, the resolution can be enhanced considerably if an ion mirror is employed.

CONCLUSIONS

In conclusion, a linear laser-ionization TOF mass spectrometer has been constructed and successfully tested, for first time in Iran, to the best of our knowledge. The instrument is promising for research and laboratory applications in applied and fundamental sciences in the field of physical, analytical and bio chemistry. In addition, the

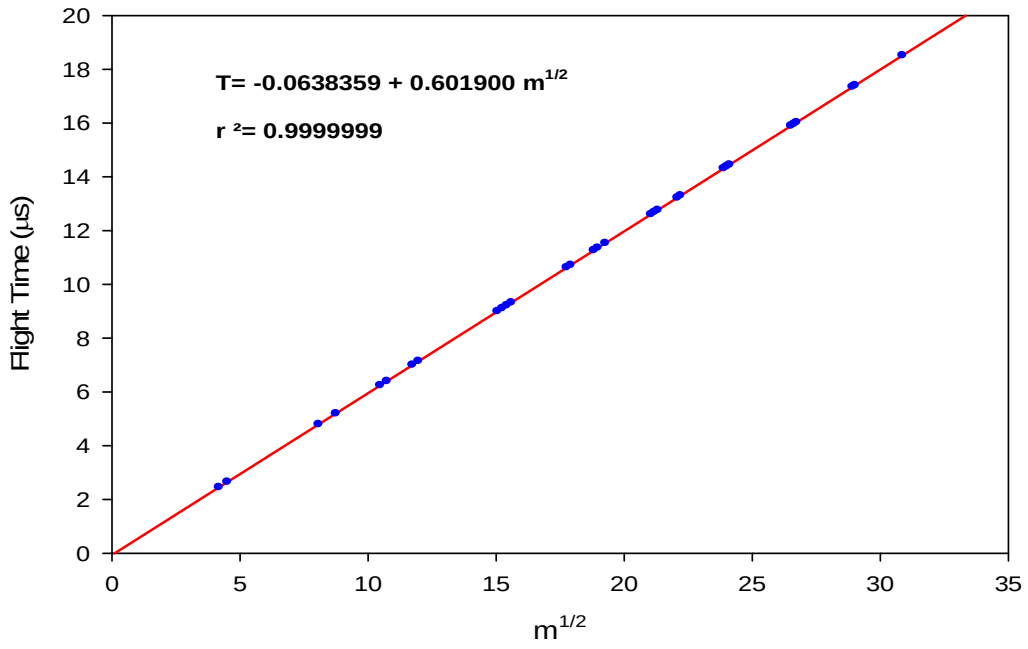

Fig. 11. Mass calibration curve in which the total flight time was plotted against the square root of mass.

Table 2. Measured and Exact Masses, as well as Mass Errors and Mass Accuracies for the Species Shown in Fig. 10

Assignment	Flight time (μs)	Measured mass	Exact mass **[10]**	Mass error (Δm)	Mass accuracy (%)
^{6}Li	4.1809	6.0157	6.0151	0.0006	0.0100
^{7}Li	4.5068	7.0164	7.0160	0.0004	0.0057
^{23}Na	8.0704	22.9803	22.9898	-0.0095	-0.0413
^{27}Al	8.7444	27.0343	26.9815	0.0528	0.1957
^{39}K	10.4750	38.9514	38.9637	-0.0123	-0.0316
^{41}K	10.7390	40.9601	40.9618	-0.0017	-0.0042
^{7}Li ($^{7}Li^{35}Cl$)	11.7330	48.9761	49.0009	-0.0248	-0.0506
^{7}Li ($^{7}Li^{37}Cl$)	11.9700	50.9931	50.9979	-0.0048	-0.0094
^{23}Na($^{23}Na^{35}Cl$)	15.0520	80.9280	80.9485	-0.0205	-0.0253
^{23}Na($^{23}Na^{37}Cl$)	15.2350	82.9219	82.9455	-0.0236	-0.0285
^{85}Rb	15.4150	84.9068	84.9118	-0.0050	-0.0059
^{87}Rb	15.5950	86.9152	86.9092	0.0060	0.0069
^{39}K ($K^{35}Cl$)	17.7570	112.8723	112.8963	-0.0240	-0.0213
^{39}K ($K^{35}Cl$)	17.9150	114.9021	114.8944	0.0077	0.0067
^{85}Rb ($^{7}Li^{35}Cl$)	18.8190	126.8632	126.8967	-0.0335	-0.0264
^{85}Rb ($^{7}Li^{37}Cl$)	18.9640	128.8368	128.8937	-0.0569	-0.0441
^{133}Cs	19.2610	132.9270	132.9054	0.0216	0.0163
^{39}K ($^{85}Rb^{35}Cl$)	21.0460	158.8555	158.8444	0.0111	0.0070
^{39}K ($^{87}Rb^{35}Cl$)	21.1780	160.8645	160.8417	0.0228	0.0141
or ^{39}K ($^{85}Rb^{37}Cl$)	//	//	160.8414	0.0231	0.0144
^{133}Cs($^{7}Li^{35}Cl$)	22.0780	174.8993	174.8903	0.0090	0.0051
^{133}Cs($^{7}Li^{37}Cl$)	22.2030	176.8949	176.8873	0.0076	0.0043
^{85}Rb ($^{85}Rb^{35}Cl$)	23.8840	204.8328	204.7925	0.0403	0.0197
^{85}Rb ($^{87}Rb^{35}Cl$)	24.0000	206.8362	206.7899	0.0463	0.0224
or ^{85}Rb ($^{85}Rb^{37}Cl$)	//	//	206.7896	0.0466	0.0225
^{85}Rb ($^{87}Rb^{37}Cl$)	24.1160	208.8493	208.7869	0.0624	0.0299
or ^{87}Rb ($^{87}Rb^{35}Cl$)	//	//	208.7872	0.0621	0.0297
^{85}Rb ($^{133}Cs^{35}Cl$)	26.5210	252.7842	252.7861	-0.0019	-0.0008
^{85}Rb ($^{133}Cs^{37}Cl$)	26.6250	254.7787	254.7831	-0.0044	-0.0017
or ^{87}Rb ($^{133}Cs^{35}Cl$)	//	//	254.7834	-0.0047	-0.0019
^{87}Rb ($^{133}Cs^{37}Cl$)	26.7290	256.7809	256.7805	0.0004	0.0002
^{133}Cs($^{133}Cs^{35}Cl$)	28.9180	300.7430	300.7797	-0.0367	-0.0122
^{133}Cs($^{133}Cs^{37}Cl$)	29.0140	302.7505	302.7767	-0.0262	-0.0087
$^{7}Li(^{133}Cs^{35}Cl)_2$	30.8640	342.7401	342.7646	-0.0245	-0.0071

instrument can be used in food science as well as industrial and health applications. These include monitoring the exhaled breath and measuring the isotope ratio, for example $^{13}CO_2/^{12}CO_2$, a biomarker for nutritional and metabolic status [13]. Furthermore, the instrument has the capability to be used for MALDI (Matrix Assisted Laser Desorption/Ionization) analysis, a very well known technique in biochemistry. If a tunable laser is used, the wavelength can be scanned over a wide range to perform resonance enhanced multi-photon ionization (REMPI) spectroscopy. The mass accuracy and resolution are acceptable for many applications. Currently, a high resolution electrospray TOF is under development. This further expands our experience and ability in technologies connected to mass spectrometry and provides the need for many researchers in Iran. The Laser-TOF instrument is patented [8] and will be commercially available in the near future.

ACKNOWLEDGEMENTS

The construction of the instrument, done by M. Tabrizchi, took three years, before its first operation. Tabrizchi would like to appreciate the hospitality, generosity and understanding of Dr. G.R. Ghorbani and Dr. H.S. Ghaziaskar in providing financial support for the material and equipments needed for building this instrument, during their administrative responsibility as president and research deputy of Isfahan University of Technology, respectively, in 2007.

REFERENCES

[1] W.C. Wiley, I.H. McLaren, Rev. Sci. Instrum. 26 (1955) 1150.

[2] R.E. Smalley, L. Wharton, D.H. Levy, Acc. Chem. Res. 10 (1977) 139.

[3] U. Boesl, R. Weinkauf, E.W. Schlag, Int. J. Mass Spectrom. Ion Proc. 112 (1992) 121.

[4] B.A. Mamyrin, V.I. Karataev, D.V. Shmikk, V.A. Zagulin, Soviet Phys. JETP 37 (1973) 45.

[5] B.A. Mamyrin, Int. J. Mass Spectrom. Ion Proc. 131 (1994) 1.

[6] R.J. Cotter, Time-of-Flight Mass Spectrometry, American Chemical Society, Washington, DC 1994.

[7] M. Tabrizchi, Multi Photon Spectroscopy of some Short-Lived Molecules, Ph.D. Thesis, University of Southampton, April 1996.

[8] M. Tabrizchi, Construction of a Laser Ionization Time-of-Flight Mass Spectrometer, Iran Patent No. 73361, 2012.

[9] http://webbook.nist.gov. 2013.

[10] M. Tabrizchi, Anal. Chem. 75 (2003) 3101.

[11] NIST: Atomic Weights and Isotopic Compositions of the Elements, 2014 http://www.nist.gov.

[12] N.E. Holden, in: Lide, D.R. (Ed.), Table of the Isotopes, CRC Handbook of Chemistry and Physics, 81st ed., CRC Press, Boca Raton, FL, 2000.

[13] D.E. Butz, S.L. Casperson, L.D. Whigham, J. Anal. At. Spectrom. 29 (2014) 594.